



HAL
open science

Unprecedented perspectives in the application of CinNapht fluorophores provided by a “Late-stage” functionalization strategy

Eléonore Tacke, Minh-Duc Hoang, Kevin Tatoueix, Benoît Keromnes, Elsa van Eslande, Philippe Durand, Gregory Pieters, Arnaud Chevalier

► To cite this version:

Eléonore Tacke, Minh-Duc Hoang, Kevin Tatoueix, Benoît Keromnes, Elsa van Eslande, et al.. Unprecedented perspectives in the application of CinNapht fluorophores provided by a “Late-stage” functionalization strategy. *Chemical Science*, 2023, 14 (22), pp.6000-6010. 10.1039/D3SC01365K . hal-04094955

HAL Id: hal-04094955

<https://hal.science/hal-04094955>

Submitted on 11 May 2023

HAL is a multi-disciplinary open access archive for the deposit and dissemination of scientific research documents, whether they are published or not. The documents may come from teaching and research institutions in France or abroad, or from public or private research centers.

L'archive ouverte pluridisciplinaire **HAL**, est destinée au dépôt et à la diffusion de documents scientifiques de niveau recherche, publiés ou non, émanant des établissements d'enseignement et de recherche français ou étrangers, des laboratoires publics ou privés.



Distributed under a Creative Commons Attribution - NonCommercial 4.0 International License

ARTICLE

Unprecedented perspectives in the application of CinNapht fluorophores provided by a “Late-stage” functionalization strategy.

Eléonore Tacke,^a Minh-Duc Hoang,^a Kevin Tatoueix,^b Benoît Keromnes,^a Elsa Van Eslande,^a Philippe Durand,^a Gregory Pieters^b and Arnaud Chevalier*^a

Received 00th January 20xx,
Accepted 00th January 20xx

DOI: 10.1039/x0xx00000x

A simple and easy-to-implement process based on a nucleophilic aromatic substitution reaction with a wide variety of nucleophiles on a fluorinated Cin-Napht is described. This process has the key advantage of introducing multiple functionalities at the very late stage, thus providing access to new applications including photostable and bioconjugatable large Stokes Shift red emitting dyes, selective organelle imaging agents, or AIEE-based wash-free lipid droplets imaging in live cells with high signal-to-noise ratio. The synthesis of bench-stable CinNapht-F has been optimized and can be reproduced in large scale, making it an easy-to-store starting material that can be used at will to prepare new molecular imaging tools.

Introduction

For decades, chemists and biochemists have been working on the development of new organic fluorophores by devising new luminescent aromatic structures. These small molecules are now commonly used for multiple applications, including fluorogenic labeling¹ or molecular probes dedicated to sensing². Nevertheless, we are still looking for the perfect dye that would meet all the criteria sought by scientists. This is a fact: the perfect dye does not exist and probably never will. Despite this, “tireless chemists” continue to devote themselves to development new fine-tuned structures that could bring precious help to biologists.^{1c} It is, therefore, essential to maintain the development of synthetic methods allowing access to an ever-increasing variety of fluorophores. Despite recent improvements through the development of new near-infrared fluorophores or the emergence of biphotonic microscopy, there remains a real advantage in using large Stokes shift red-emitting fluorophores. They have the key advantage of avoiding spectral overlap, and therefore allow to optimize the acquisition parameters during imaging experiments. The synthesis of such fluorophores is extensively studied, thus several approaches have been elaborated providing multiple original fluorophores.³ In this context, we have recently reported a Naphthalimide-Cinnoline hybrid dye called CinNapht which has proven to be useful in imaging experiments.⁴ We showed that the modification of the amine

moiety allows to adjust the photophysical properties.⁵ This feature makes CinNaphts versatile platforms for biological or photophysical purposes. However variation of the electro-donating aniline moiety in the fluorophore, requires a complete re-synthesis of the dye, starting from the suitable pinacolborane *meta*-substituted aniline (Fig. 1, top), which often needs to be prepared. This is the main limitation of the previous synthetic approach, which resulted in a restriction in both the number and variety of accessible CinNaphts analogues. In addition, the last step of the synthetic process, based on SEAR (electrophilic aromatic substitution) type reaction of an intermediate diazonium salt, leads to the formation of *ortho* and fluorescent *para* regioisomers. Even though the *para* isomer was the major product, its isolation requires purification steps which inevitably causes reduced reaction yields.⁴

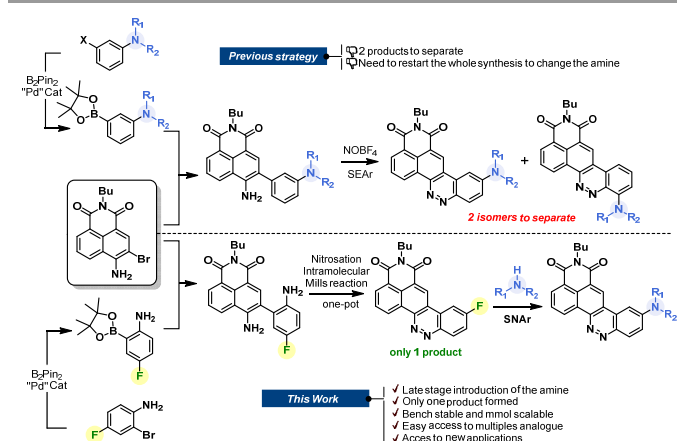


Figure 1: Description of the new CinNapht synthesis strategy and highlighting of improvements.

Based on these considerations, we sought to design a robust and efficient synthesis procedure allowing to unlock the real potential of CinNaphts for fluorescence imaging. In this paper,

^a Université Paris-Saclay, CNRS, Institut de Chimie des Substances Naturelles, UPR 2301, 91198, Gif-sur-Yvette, France.

^b Département Médicaments et Technologies pour la Santé (DMTS), SCBM, Université Paris-Saclay, CEA, INRAE, 91191 Gif-sur-Yvette, France.

†Electronic Supplementary Information (ESI) available: [details of any supplementary information available should be included here]. See DOI: 10.1039/x0xx00000x



we propose a synthetic pathway allowing to introduce various nucleophilic moieties at the very end of the synthesis through nucleophilic aromatic substitution (SNAr). The late-stage strategy is an astute way to conveniently incorporate electron donors on a fluorescent scaffold. Already illustrated in the literature, the previously described examples are mostly based on a Buchwald palladium-catalyzed amination reaction on aromatic triflate or halide.⁶ This strategy led to multiple examples of fluorescent probes with improved photophysical properties⁷ and opening new perspective of bioanalytical purposes.⁸ Despite the fact that it avoids the use of metal, SNAr has rarely been used in fluorophore postamination strategies,⁹ and has never been considered for the final functionalization of CinNaphts. In this paper, we propose a robust synthetic route for the large-scale preparation of an aryl fluoride derivative of CinNapht that can undergo a nucleophilic substitution reaction with a wide variety of nucleophiles to provide simple access to a broad range of fluorophores, including bioconjugatable analogs, CinNapht with improved photostability and unprecedented organelle CinNapht-based markers.

Results and discussions

Large scale synthesis of CinNapht-F and study of its reactivity through SNAr reactions

We started by designing a synthetic route for the preparation of a fluorinated CinNapht (CinNapht-F, **4**). The major issue to be managed was the formation of the N=N double bond constituting the cinnoline part (Fig. 1). In addition to the fact that it leads to the formation of two isomers, the strategy initially employed for the synthesis of these fluorophores, uses an aromatic electrophilic substitution reaction requiring enriched aromatic unit. As we had anticipated, the implementation of this strategy for the synthesis of a fluorinated fluorophore gave particularly poor results, probably due to the low electronic enrichment of the fluorinated aromatic moiety, which did not allow for a good reactivity with SEAr.

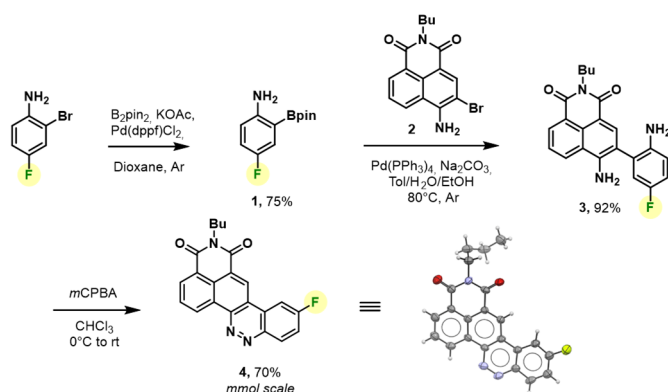


Figure 2. mmol scalable synthesis and X-ray diffraction structure of bench stable CinNapht-F **4**.

We thus revised the synthetic route in order to allow the formation of azobenzene by an intramolecular Nitrosation/Mills reaction one-pot process, which would therefore not require an

electron rich fluorinated aromatic ring. Thus, the aromatic bis adduct **3** was prepared by Suzuki-Miyaura cross-coupling reaction catalysed by Pd(PPh₃)₄ in very good yield of 92% starting from the molecule **2**. This intermediate was then treated with *m*CPBA to form the desired derivative in 70% yield. The structure of **4** was unambiguously confirmed by NMR, HRMS and an X-ray diffraction pattern was also obtained. This reaction was shown to be reproducible and implementable on a large scale (2-3 mmols) making it a robust process for the synthesis of CinNapht-F. To our delight, this fluorinated dye was found to be highly stable over months, without any specific storage conditions. We then studied the reactivity of CinNapht-F in a model SNAr reaction using *n*-Butylamine as nucleophile (Table1).

Table 1 Methodological study of SNAr reaction using *n*-Butylamine

Entry	Solvent ^a	Base ^b	Temp (°C)	Time (h)	HPLC Yield ^c
1	DMF	Na ₂ CO ₃	100	24	95
2	DMF	K ₂ CO ₃	100	24	87
3	DMF	Cs ₂ CO ₃	100	24	68
4	DMF	K ₃ PO ₄	100	24	83
5	DMF	K ₂ HPO ₄	100	24	86
6	DMF	NaHCO ₃	100	24	95
7	DMF	KOH	100	24	31
8	DMF	AcOK	100	24	80
9	DMF	<i>t</i> BuOK	100	24	13
10	CH ₃ CN	NaHCO ₃	80	24	/ ^d
11	DMSO	NaHCO ₃	100	24	91
12	Dioxane	NaHCO ₃	100	24	/ ^d
13	NMP	NaHCO ₃	100	24	96
14	DCE	NaHCO ₃	70	24	3
15	Tol	NaHCO ₃	100	24	/ ^d
16	DMF	NaHCO ₃	60	24	60
17	DMF	NaHCO ₃	25	24	0
18	DMF	NaHCO ₃	100	24	85 ^e
19	DMF	NaHCO ₃	100	0.5	80
20	DMF	NaHCO ₃	100	1	97
21	DMF	NaHCO ₃	100	4	96

^aDry solvent were used, ^b4.0 equivalents of base were used. ^cCalculated on Max Plot PDA chromatogram. ^dNot determined due to lack of solubility. ^eUsing 1.05 equivalent of *n*BuNH₂.

Butylamine was reacted with CinNapht-F **4** under a range of conditions. Lines 1 to 9 in Table 1 show that in DMF while heating, the reaction tolerates most of the bases we could try, with the exception of slightly stronger bases such as *t*BuOK or NaOH (lines 7 and 9). In the same way, the aprotic polar solvents allowing the solubilization of the starting CinNapht, are on the whole usable with no particular variability for this reaction. The lack of conversions observed in some cases was mainly due to insolubility of the starting substrate (lines 10, 12, 14 and 15). We could observe that the reaction also works at 60 °C and after changing the number of equivalents and studying the reaction



time, we finally established that, in the case of *n*-Butylamine, 1h of reaction at 100 °C in DMF using NaHCO₃ as base, provided the best result with 97% of HPLC Yield. We next conducted further studies to evaluate the scope of this reaction. A wide variety of nucleophiles, exhibiting different reactivity, were tested with variable isolated yields summarized Figure 3. Aliphatic (**5a–5c**) and benzylic amines (**5d**, **5e**), whether primary or secondary, gave good results with isolated yields reaching up to 95%. α -type nucleophiles were also investigated. While methyl hydrazine showed good result with 80% of isolated CinNapht **5g**, methoxyamine was surprisingly found unreactive. Other oxyamines were tested but none of them led to SNAr reaction product (data not shown).

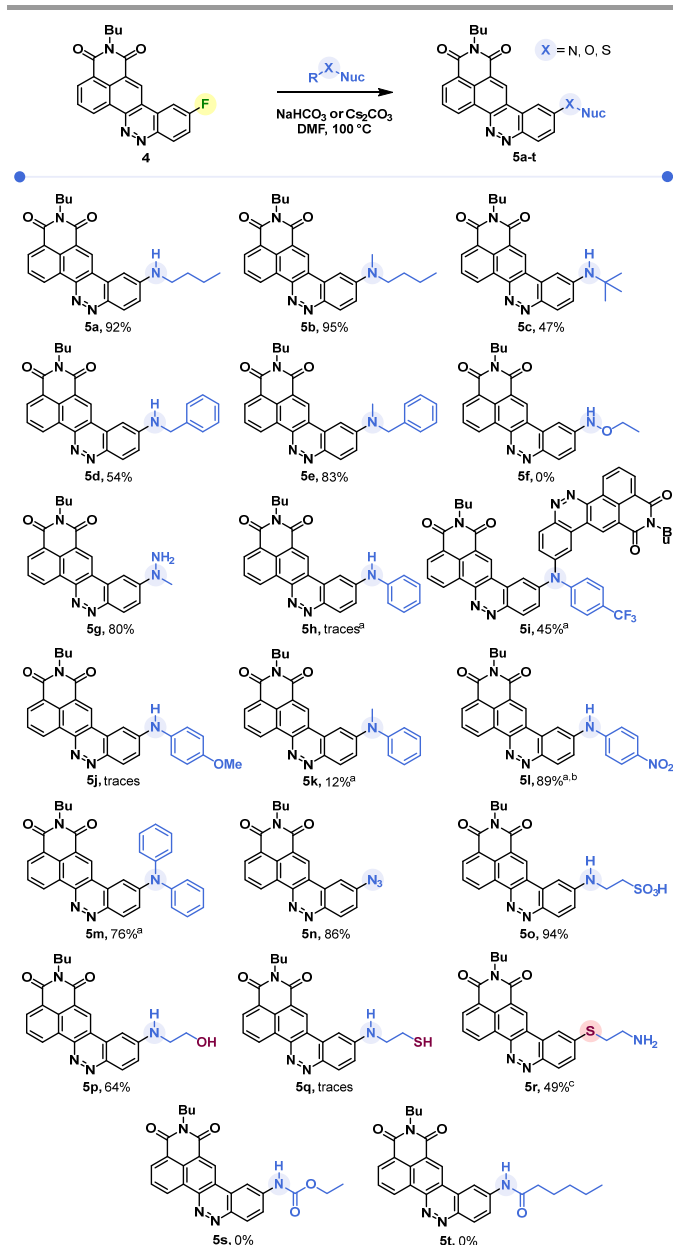


Figure 3. Scope of the reaction of SNAr on CinNapht-F. ^aCs₂CO₃ used as a base. ^bHPLC Yield based on Max Plot chromatogram. ^cIsolated yields by reaction of thioethanolamine. (nuc = nucleophile)

The reactivity of aromatic amines was also studied (**5h–5m**). Either no reaction or very low conversion were observed using

NaHCO₃ as a base. Nevertheless, we were able to obtain the product of diphenylamine addition by changing the base to Cs₂CO₃. Interestingly, in the meantime no conversion was noticed with Na₂CO₃ and only poor conversion was noticed after one night using K₂CO₃ (Fig. S1). In order to better understand this selectivity of caesium carbonate, we performed two additional experiments (Fig. S1). The addition of crown ether (15-C-5) to the reaction in order to increase both the solubility and the basicity of the carbonate did not improve the reactivity of the diphenylaniline and no product was observed. In the meantime, the addition of 1 equivalent of CsF led to a very good conversion (See Fig S1, line 5). We also noticed that a supplementation with caesium fluoride using NaHCO₃ led to a significant conversion, demonstrating that caesium cation plays a key role in the improvement of aromatic amines reactivity. Thus, using Cs₂CO₃, we studied the reactivity of aromatic aniline with variable electronic enrichments (**5i** to **5m**). Good conversion was observed in most of the case (**5i**, **5k**, **5l** and **5m**) and pure Cinnaphts were isolated with yields ranging from 12% to 77%. Despite its good reactivity (see crude mixture chromatogram Fig S2), we failed in trying to isolate CinNapht **5l** as a pure compound, thus only HPLC conversion yield of 89% can be given. Unfortunately, despite the use of caesium carbonate none of the CinNaphts **5h** (aniline) and **5j** (*para*-methoxyaniline) could be isolated, and only traces of the products were observed. Surprisingly, the reaction of *para*-trifluoromethylaniline led to the formation of a dimer **5i**. This could be explained by the formation of a mono-addition product whose proton is acidic enough to allow deprotonation by caesium carbonate. This results in the formation of a much more reactive anion which will react preferentially to generate the dimer **5i**. All together, these results show that the implementation of the reaction with aromatic amines using caesium carbonate as a base must be considered carefully. Sodium azide can also be used for this reaction providing azido CinNapht **5n** with a good yield of 86%. This new derivative was thought to constitute a good candidate for fluorogenic click reactions¹⁰, radiation activation or sensing of thiols¹¹ for example. Unfortunately, compound **5n** was found to be unstable, especially in aqueous environment in which we could quickly observe the formation of the fluorescent reduction product (see Fig. S3). These results were confirmed by the appearance of a non-specific fluorescent signal in cells during confocal microscopy experiments. Moreover, the product of SPAAC reaction between **5n** and DBCO turned out to be not fluorescent, preventing its use in a fluorogenic click reaction (See Fig S4). This disappointing result leads us to warn against the use of the aryl azide **5n** for fluorogenic applications in biological media. The competition between the amine and other nucleophilic functions such as an alcohol or a thiol was also studied. While exclusive amine addition was observed in the case of ethanolamine (**5p**), a preferred thiol addition was witnessed using thioethanolamine resulting in the formation of product **5q** in line with the higher nucleophilicity of the thiol compared to the primary amine substructures. The product of amine addition may be observed in trace amounts, but exclusively under its oxidized disulphide form. This particular



reactivity of thiols on aromatic fluorides of fluorophores derivatives could thus give access to sulfide derivatives of fluorophores which can be used for ROS sensing such as hypochloric acid. This result can thus represent a source of inspiration in this field.¹² Finally, our attempts to introduce carbamides (**5s**) or primary amides (**5u**) were unsuccessful which further defines the limitation of this reaction, which nevertheless allows the introduction of a very broad range of amines.

Synthesis of original CinNaphts for new applications

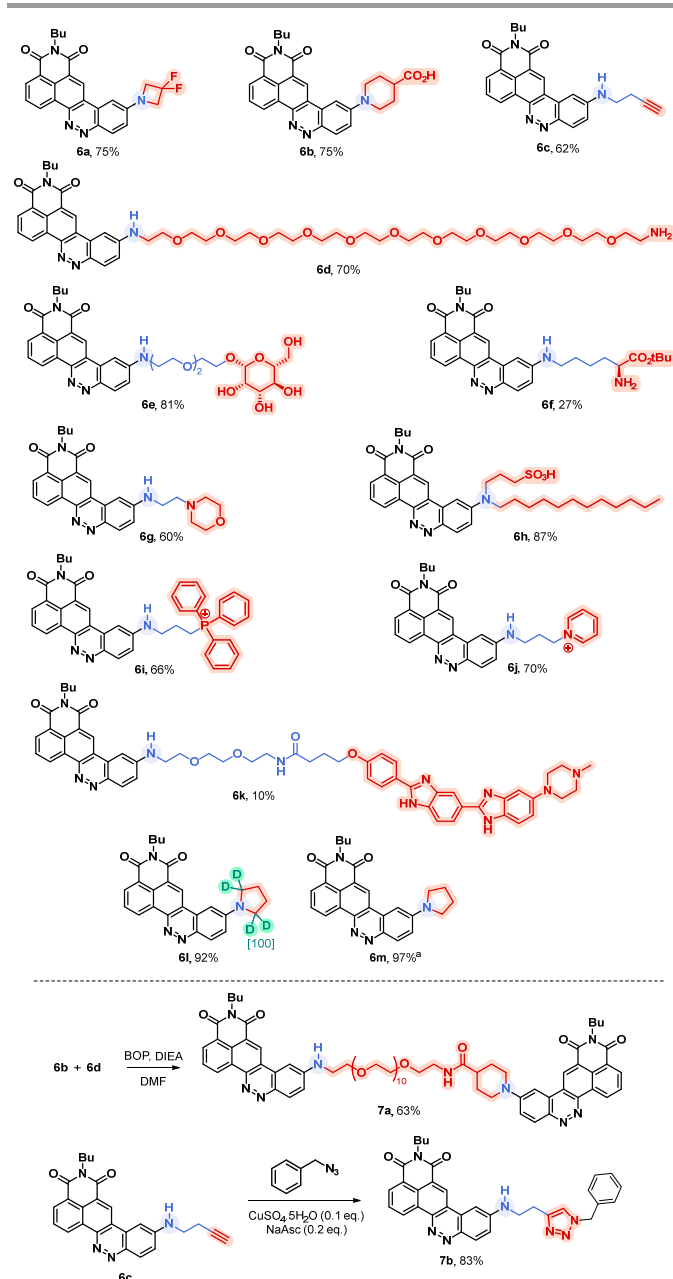


Figure 4. Examples of accessible original CinNaphts using SNAr late-stage functionalization with isolated yields. ^aCompound described previously⁵ and accessible thanks to the SNAr late-stage functionalization

Considering this remarkable versatility of the SNAr reaction we studied the introduction of more complex amines in order to generate more sophisticated fluorophores, dedicated to new

applications. Some chosen examples are presented in the Figure 3. First, We successfully introduced a difluoroazetidine moiety already reported to induce slight hypochromic shift of both absorption and emission wavelengths that we could verify also with our CinNapht.^{7a} Then we incorporated chemical functions that could allow the bioconjugation of CinNaphts. Disappointingly, the addition of glycine or sarcosine to CinNapht-F **4** failed, preventing its functionalisation by a carboxylic acid. We countered this by resorting to isonipecotic acid and obtained the CinNapht **6b** in a good yield of 60% without any prior protection of the carboxylic function. We also prepared a primary amine derivative **6d** that presents the particularity to have a PEG-10 linker separating the CinNapht from the amine function. Note that, by reacting these two CinNaphts **6b** and **6d** using BOP reagent, we easily obtained the CinNapht dimer **7a** (Fig. 4, bottom) by amide bond formation in a good isolated yield of 63%. This additional result confirmed the potential use of both the acidic derivative **6b** and the amine derivative **6d** in amidation type reactions. An alkyne derivative of CinNapht (**6c**) was also obtained in good yield and its reactivity with azide in “Click” CuAAC reaction¹³ was demonstrated by reacting it with benzyl azide using copper sulfate (0.1 eq) and sodium ascorbate (0.2 equiv.). The 1,4 disubstituted triazol adduct **7b** was isolated with 83% yield, attesting CinNapht **6c** as a potent dye for fluorescent labelling using CuAAC type Click reaction. Keeping in mind the selectivity of the amine addition over hydroxyl moiety (Fig. 3, **5p**), we tried to use more complex poly-alcohol units such as sugars. Thus, a modified manose was prepared by introducing a free amine triethylene glycol linker on the anomeric position (See compounds **8** and **9** in Supporting Information). This was reacted with CinNapht-F **4** to obtain a CinNapht-Manose **6e** derivative in 81% yield. It is noteworthy that no protection of the hydroxyl groups of the mannose was required for this reaction, which would never have been conceivable with the reported access to CinNaphts. The amino acid derivative of CinNapht (**6f**) was also prepared using Fmoc-Lys-OtBu as nucleophile partner for SNAr reaction followed by the followed removal of the Fmoc protecting group. The *t*Bu protected CinNapht **6f** was isolated in one step with a moderate yield of 27%. In order to reach new application in cell imaging, we thought that CinNapht-F could constitute an easy to functionalize building block, allowing the introduction of organelle targeting functions. We started by introducing a morpholine¹⁴ moiety that led to a lysosome accumulating CinNapht (**6g**) with 60% yield. The introduction of a zwitterionic lypophilic amine (Cf. SI file, compound **10**), enables to obtain the CinNapht **6h**, thought for cell plasma membrane labelling, and isolated with 87% yield.¹⁵ We also introduced with good yield both a triphenylphosphonium (**6i**) or a pyridinium moiety (**6j**) with the idea to target mitochondria.¹⁶ The possibility of introducing sophisticated amines at the very late stage of the synthetic process led us also to consider the introduction an amine derivative of Hoechst.¹⁷ This led to the CinNapht (**6o**) with 10% yield, designed for imaging the nucleus of the cells. Finally, we investigated the access to deuterated CinNaphts. This was motivated by recent works from Lavis lab suggesting



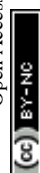
that the deuteration of the donating amines in fluorophores can improve its photophysical performances^{7b}, and further confirmed by a recent study published by Lehmann, Broichhagen and coworkers.¹⁸ Thus, introduction of

regioselectively α -deuterated pyrrolidine¹⁹ was performed and led to **6l** with very good isolated yield of 92%. This came to complete a set of new fluorophores whom photophysical properties were investigated

Table 2. Photophysical properties of CinNapht prepared through SNAr

Dye	Solvent	λ_{\max} Abs ^a (nm)	ϵ_{\max} ^b (M ⁻¹ .cm ⁻¹)	λ_{\max} Em (nm)	Stokes Shift ^c (cm ⁻¹)	QY _{Fl} ^e	Brightness $\epsilon_{\max} \times$ QY _{Fl}
4	CHCl ₃	359	18 292	/	/	/	NA
5a	CHCl ₃	466	8 111	581	4 248	0.15	1 217
5b	CHCl ₃	498	12 099	582	2 898	0.29	3 509
5c	CHCl ₃	471	6 731	576	3 870	0.15	1 010
5d	CHCl ₃	456	11 495	576	4 569	0.11	1 264
5e	CHCl ₃	484	9 180	570	3 117	0.21	1 928
5g	CHCl ₃	470	12 916	583	4 124	<0.01	ND
5i	CHCl ₃	476	12 217	554	2 958	0.08	977
5k	CHCl ₃	482	11 055	630	4 874	<0.01	ND
5m	CHCl ₃	496	15 078	665	5124	0.04	603
5n	CHCl ₃	378	8 148	/	/	/	NA
5o	DMSO	485	3 143	665	5581	0.05	157
5p	CHCl ₃	459	11 808	590	4837	0.15	1 771
5r	CHCl ₃	403	8 312	/	/	/	NA
6a	CHCl ₃	446	4 765	554	4 371	0.05	238
	PBS + 5%BSA	471	ND	560	ND	< 0.01	ND
6b	DMSO	477	4 961	682	6 302	0.17	843
	PBS + 5%BSA	508	3 615	610	3 292	0.02	072
6c	CHCl ₃	456	9 374	570	4 386	0.09	844
	PBS + 5%BSA	490	8 223	608	3 961	0.02	164
6d	CHCl ₃	470	9 193	603	4 693	0.19	1 747
	PBS + 5%BSA	493	7 280	611	3 917	0.02	146
6e	CHCl ₃	471	4 866	592	4 340	0.17	827
	DMSO	486	6 441	655	5 309	0.18	1 159
	PBS + 5%BSA	479	5 088	585	3 783	0.02	102
6f	CHCl ₃	468	11 265	586	4 303	0.19	2 140
	PBS + 5%BSA	477	9 970	584	3 841	0.02	199
6g	CHCl ₃	465	2 144	570	3 962	0.10	214
	DMSO	485	2 729	659	5 444	0.13	355
	PBS + 5%BSA	485	2 177	575	3 227	0.02	44
6h	CHCl ₃	520	3 069	615	2 971	0.32	982
	DMSO	511	4 639	677	4 798	0.28	1 299
	PBS + 5%BSA	513	4 374	620	3 364	0.05	219
6i	CHCl ₃	487	2 155	594	3 699	0.23	496
	DMSO	484	3 432	651	5 300	0.11	377
	PBS + 5%BSA	485	2 977	593	3 755	0.02	60
6j	DMSO	480	9 017	652	5 496	0.16	1 443
	PBS + 5%BSA	493	7 946	619	4 129	0.02	159
6k	DMSO	486	4 763	660	5 425	0.18	857
	PBS + 5%BSA	491	3 026	ND	ND	< 0.01	ND
6l	CHCl ₃	502	10 926	590	2 971	0.33	3 606
	PBS + 5%BSA	515	6 830	628	3 494	0.03	205
6m	CHCl ₃	502 ^d	9 296	592 ^d	3 028 ^c	0.33 ^{c,d}	3 068
	PBS + 5%BSA	515 ^d	3 646 ^d	612 ^d	3 078 ^d	0.04 ^d	146
7a	CHCl ₃	470	26 337	584	4 153	0.12	3 160
	DMSO	485	20 611	667	5 626	0.14	2 885
7b	CHCl ₃	463	5 209	584	4 475	0.11	573
DCM	EtOH	467	42 000	622	5 336	0.43	18 060
ATTO 490LS	PBS Buffer	495	40 000	658	5 004	0.30	12 000
DyLight 515-LS		515	50 000	650	4 032	/	/

^aValues corresponding to S0–S1 transition but strong S0–S2 transition is also observed (see Fig. S3 to S5), ^bMolar extinction coefficient related to S0–S1 transition (see Fig. S8 to S9). ^cRelative QY determined at 25 °C using 4-(Dicyanomethylene)-2-methyl-6-(4-dimethylaminostyryl)-4H-pyran, "DCM" (QY = 0.43 in EtOH)²⁰, ^dCompound 6n was previously described⁵, but photophysical characterization was reproduced using the same fluorimeter as for other CinNaphts in order to enable more accurate comparison.



ARTICLE

Photophysical properties

The photophysical properties of all the synthesized analogues have been investigated. The absorption, excitation and emission spectra were recorded at 25 °C in CHCl₃. We determined the $\lambda_{\text{max}}^{\text{Em}}$ and $\lambda_{\text{max}}^{\text{Abs}}$ as well as the molar extinction coefficient (ϵ_{max}) and the fluorescence quantum yields (Q_{F}). The results of this study are reported in Table 2. A moderate modulation of the absorption maxima, centred mainly between 465 and 500 nm were observed depending on the nature of the amine. We can nevertheless observe that a methylation of the amine generates an expected bathochromic shift of the absorption maximum, which is located here at about 30 nm as can be seen by comparing the derivative **5a** to the derivative **5b**. This seems to be independent of the nature of the amine, since the same type of behaviour is observed for benzyl amines derivatives **5d** and **5e**. Arylation induces a slight bathochromic shift especially for the diphenylamine derivative **5m** whose absorption maximum reaches 496 nm. Note also that the thioether derivative **5r** displays a particularly blue-shifted absorption maximum. Regarding the fluorescent properties of these compounds, several variations can be highlighted. First of all, the use of a secondary amine does not seem to generate a particular shift of the emission wavelength with almost identical maxima for compounds **5a** and **5b** for instance. On the other hand, this substitution seems to provide an improvement of the fluorescence efficiency with a doubled fluorescence quantum yields for **5b** compared to **5a**, also observed for **5d** and **5e**. This may be attributed to more hindered amine substituent preventing from non radiative deexcitation due to C-N bond rotation. We can thus suggest that the introduction of a secondary amine allows to improve the fluorescence quantum yield, but induces a decrease of the Stokes shift. The use of an α -nucleophile or aromatic seems to be deleterious for the fluorescence since negligible fluorescence was observed for the derivatives **5g** and **5k**. Also a complete absence of fluorescence for the azide compound **5n** as well as the thioether **5r** was noticed. The set of fluorophores (**6a-n**) that have been prepared for potential new applications, including use in biological systems, have also been characterized. For these, the set of measurements in CHCl₃ was completed by additional measurements in a PBS buffer containing 5% BSA. The results obtained in CHCl₃ are in most cases comparable with the results presented previously, i.e. an absorption centred between 470 and 500 nm and an emission observed around 580 nm. Only compound **6h** displays a singular absorption maximum, slightly red-shifted and centered at 520 nm and an emission at 615 nm. Note that the ICT nature of the fluorescence mechanism involved for CinNaphts results in a pronounced bathochromic shift of the emission maximum in polar solvents.⁴ Thus for compounds **6b**, **6j** and **6k** that were not soluble in chloroform, and for which we resorted to DMSO, we notice that emissions are particularly red-shifted. A significant example of this phenomenon is the isonipecotic

acid derivative **6b** which has an emission maximum measured at 682 nm for a Stokes shift of 6302 cm⁻¹ and a Q_{F} = 0.17. Compound **6a** incorporating a difluoroazetidone unit is distinct in that it was proposed to slightly blue-shift the absorption and emission maxima. The result is consistent with the literature as it shows the lowest maxima of all fluorophores ($\lambda_{\text{max}}^{\text{Abs}}/\text{Em}$ = 446/554 nm). The quantum yields of these fluorophores measured in organic solvents vary little with values close to 20% which is in accordance with the values previously described for this type of fluorophores.⁵ However **6a** showed an erosion of Q_{F} that had not been particularly observed in the literature. It seems that the introduction of a difluoroazetidone allows the hypsochromic tuning of the emission wavelength, but causes a decrease of the fluorescence efficiency for CinNapht dyes. The best values are obtained for the compound **6l** and **6m**, with values above 30%, in accordance with those observed for the corresponding non-deuterated derivative. The weak solubility of CinNaphts in PBS buffer leads to a low fluorescence emission and could not allow the study of their photophysical properties. Nevertheless, by supplementing the PBS buffer with 5% BSA, the fluorescent behavior of CinNaphts in aqueous medium can be evaluated. In general, we also observed a drastic decrease of the fluorescence efficiency in the PBS + 5% BSA buffer with values mainly from 2 to 5%, which is expected and consistent with the lack of solubility that we noticed, also characterized by a low molar extinction coefficient. The set of CinNaphts proposed in this article exhibit promising photophysical properties which nevertheless remain below the equivalent commercially available ones (DCM²⁰, ATTO 490LS²¹ or DyLight 515-LS²²). However, thanks to the wide variety of CinNapht structures, they constitute valuable tools that allow considering multiple applications

TD-DFT Calculation

In order to better understand the variability of photophysical properties observed with these novel CinNaphts, DFT and TD-DFT calculations were conducted. The ground state geometries of representative compounds (**5a**, **5b**, **5d**, **5e**, **5m**, **5n**, **5r**, **6l**) were first optimized using B3LYP-D3(BJ)/6-311G(d,p)/IEF-PCM(CHCl₃) level of calculation followed by a frequency calculation to confirm the convergence to a local minimum. Then, TDDFT calculations were performed at the PBE1PBE/6-311G(d,p) level of theory with a IEF-PCM solvation model for CHCl₃. Absorption energies and oscillator strengths of their first 12 vertical excitations were calculated and used to simulate the UV spectra (SI page 112-116). The use of the PBE1PBE/6-311G(d,p) level of theory with the IEF-PCM solvation model has allowed to estimate relatively well the $\lambda_{\text{max}}^{\text{Abs}}$ (Fig. 5) and to furnish simulated UV spectra in very good agreement with the experimental ones (Table in Fig. 5). The observed redshift of the $\lambda_{\text{max}}^{\text{Abs}}$ of **5b** compared to **5a** is rather well reproduced by the calculation (experimental : 32 nm ; calculated 21 nm) and in line with the difference in terms of HOMO-LUMO gaps calculated for both



molecules (3.05 eV for **5a** and 2.92 for **5b**). As expected, for all of the emissive CinNaphts, the first excitation mainly involves a HOMO-LUMO π - π^* transition (contribution 99%). The frontier orbitals distributions for all the emissive compounds confirm the charge transfer character of the first excited state with an HOMO coefficients located around the alkylamine substituent whereas the LUMO coefficients are closer to the naphthalimide substructure (see Sup. Info page 113-116 for FMOs distributions).

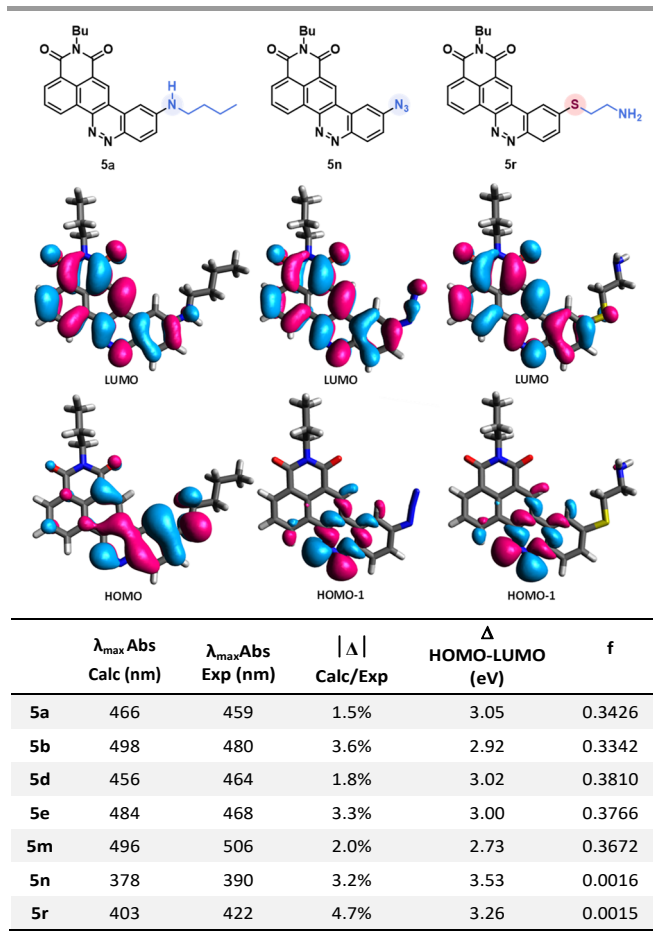


Figure 5. Rationalization through quantum mechanical calculations. Frontiers molecular orbitals of **5a**, **5n** and **5r** highlighting the HOMO nature difference. Table: Comparison between experimental and theoretical results including oscillator strength (f).

Interestingly, for non-emissive CinNaphts **5n** and **5r**, the TDFT calculations predict a first excitation involving mainly a HOMO-1 \rightarrow LUMO transition, corresponding to n - π^* type of transition, the HOMO-1 being located mainly on the nitrogen atoms of the cinnoline moiety (see SI page 115). This result may explain the absence of fluorescence for CinNaphts **5n** and **5r**.

Influence of Deuteration in photobleaching resistance

Encouraged by the results published by Lavis' group^{7b} we investigated the influence of the deuteration of the donating amine on the photophysical properties of our compounds. First, the emission spectra, quantum yields and molar absorbance coefficients were determined for compounds **6l** (Deuterated) and **6m** (not deuterated). The values obtained and reported in Figure 6d indicate a negligible influence on both the absorption and emission maxima, which is consistent with the literature. On the other hand, while

previous works demonstrate a clear benefit on the quantum yield, no obvious improvement has been noticed in our case. This leads us to carefully consider the deuteration strategy when it comes to optimizing the fluorescence efficiency. Nonetheless, Absorption coefficient values were found to be significantly enhanced in favour of the deuterated compound, which is a trend also observed by Lavis group. We then performed bleaching experiments to evaluate the photochemical resistance of our compounds. Both of the two CinNaphts were irradiated at 470 nm using a Teleopto device (See SI file, p45), and recording of both absorbance and emission spectra were performed every 30 min. Every experiment was performed in triplicate. The Figure 6b depicts a decrease of the emission intensity concomitant with a slight hypsochromic shift of the emission maxima. This evolution is significantly slower for **6l** than for **6m** testifying to a substantial improvement of the photochemical resistance brought by the regioselective insertion of deuterium atoms to the pyrrolidine moiety. The slight hypsochromatic shift in both the emission spectrum and the absorption band over the time (Fig. 6b and 6c) suggests a photochemical degradation partly characterized by dealkylation of the pyrrolidine nitrogen atom.

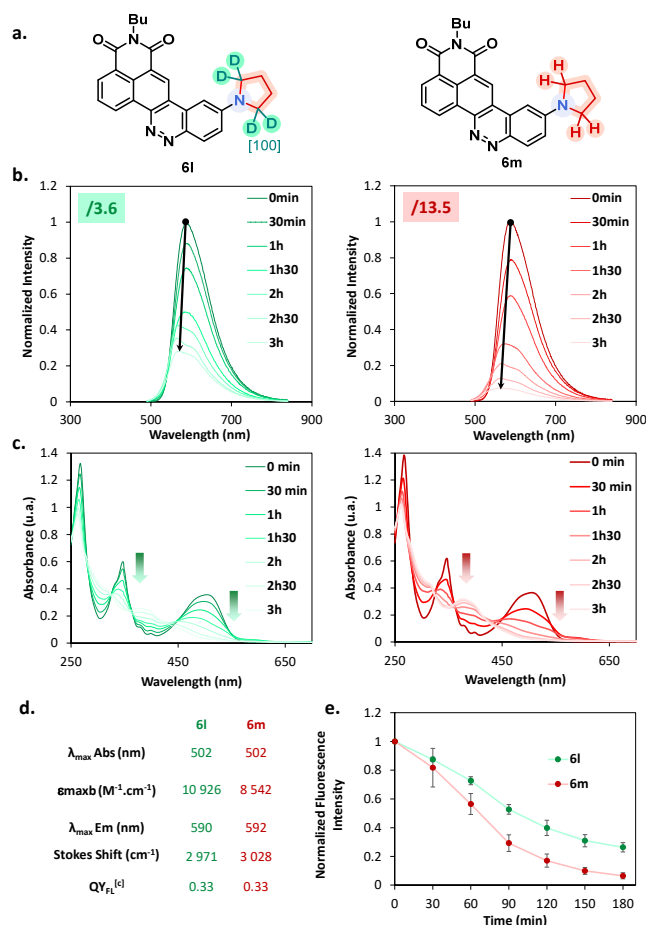


Figure 6. Influence of deuteration of pyrrolidine. a. Structures of deuterated CinNapht **6l** and non-deuterated CinNapht **6m**. b. Normalized fluorescence spectra of compounds **6l** and **6m** in $CHCl_3$ at 25°C every 30 min over 3h of irradiation at 470 nm. c. Absorbance spectra of compounds **6l** and **6m** in $CHCl_3$ at 25°C every 30 min over 3h of irradiation at 470 nm. d. Table of comparison of photophysical characteristics of CinNaphts **6l** and **6m**. e. Comparison between fluorescence intensity decline over the time after irradiation at 470 nm.



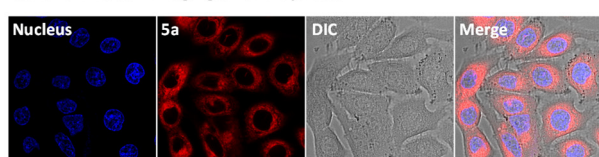
This is in accordance with Grimm and co-workers proposal^{17b} on the base of what we proposed a similar degradation mechanism (see Fig. S8). The LCMS analyses performed during the photobleaching experiment demonstrate the appearance of intermediates over time that supports the suggested mechanism. Thus, we can reasonably argue that a primary kinetic isotope effect induced by the incorporation of deuterium atoms in the α -position of the nitrogen (main site of the photobleaching degradation is the crucial point in the increased stability of CinNapht **6m**). This difference leads to a more difficult homolytic rupture of the C-D bond as a result of the photo-oxidation step, and consequently to a slower photochemical degradation of the deuterated dye. The introduction of a deuterated amine at the very end of the reaction is therefore an obvious advantage in the quest for photostable fluorophores. Considering the expensive cost of commercial deuterated amines, this strategy allows an undeniable cost economy compared to the use of

deuterated compounds at the beginning of the synthesis, which would require more material. We also studied the behavior of these two fluorophores during confocal microscopy experiments, but have not observed any obvious gain from the deuteration of our CinNaphts (data not shown). Therefore, we can state that in the case of our CinNaphts, alpha deuteration improves the absorption coefficient and is beneficial for the resistance to photobleaching, but does not allow any other improvement, either in terms of fluorescence efficiency or cell imaging.

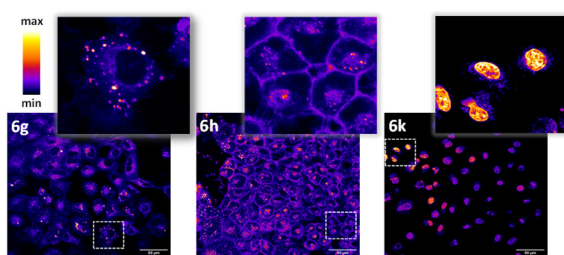
Imaging of organelles in A549 living cells

A set of fluorophores was incubated with living A459 cells then imaged with confocal microscopy experiments. We first looked at the model fluorophore **5a** and noticed that the dyes enters efficiently in the cell without needing any pre-treatment.

a. A549 vive cell imaging of CinNapht 5a



b. Subcellular compartmentalization of CinNaphts **6g**, **6h** and **6k** during A549 live cell imaging experiments



c. Colocalization experiments with CinNaphts **6g**, **6h** and **6k**

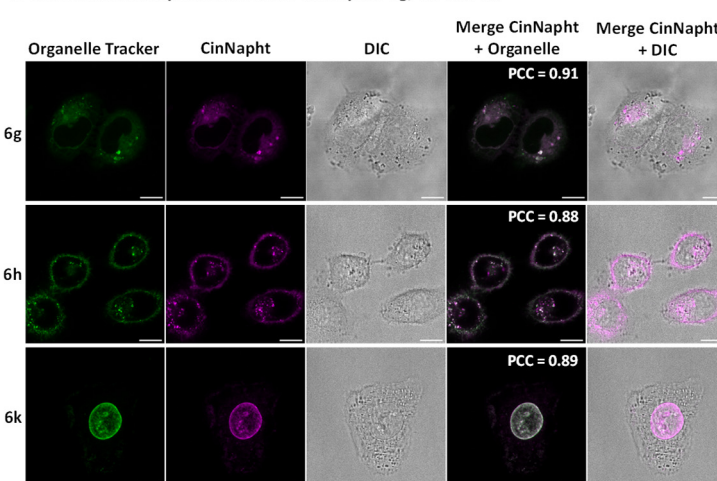


Figure 7. Confocal microscopic images of live A549 Cancer cells treated CinNaphts. a. Imaging of CinNaphts **5a** using a 63x oil immersion objective, nucleus was stained with Hoechst 33342, 1 μ g/mL for 20 min at 37 °C (λ_{Exc} : 405 nm, λ_{Em} : 425 to 500 nm), CinNapht **5a** incubated at 1 μ M for 3 h at 37 °C (λ_{Exc} : 470 nm, λ_{Em} : 550 to 700 nm). Scale bar 20 μ M. b. Subcellular localization of CinNaphts using a 63x oil immersion objective, CinNapht were incubated at 1 μ M for 3 h at 37 °C, **6g** (λ_{Exc} : 470 nm, λ_{Em} : 500 to 700 nm), **6h** (λ_{Exc} : 490 nm, λ_{Em} : 510 to 720 nm), **6k** (λ_{Exc} : 470 nm, λ_{Em} : 500 to 700 nm) Scale Bar: 50 μ M. c. Colocalization experiments. CinNapht were incubated at 1 μ M for 3 h at 37 °C, then organelles trackers were added using procedure suggested by the Biotium company (Cf Sup. Info.). **6g** (λ_{Exc} : 470 nm, λ_{Em} : 550 to 700 nm) colocalized with LysoView™ 405 (λ_{Exc} : 405 nm, λ_{Em} : 425 to 500 nm), **6h** (λ_{Exc} : 470 nm, λ_{Em} : 550 to 700 nm) colocalized with CellBrite® Green (Neuro-DiO) (λ_{Exc} : 470 nm, λ_{Em} : 490 to 530 nm), **6k** (λ_{Exc} : 470 nm, λ_{Em} : 550 to 700 nm) colocalized with NucSpot® Live 488 Nuclear Stain (λ_{Exc} : 470 nm, λ_{Em} : 490 to 530 nm). Pearson Correlation Coefficient (PCC) were calculated using JACoP plugin of ImageJ software. Scale bars 10 μ M.

The images depicted in Figure 7a also indicated that no significant compartmentalization of the dye was observed, which is consistent with the structure of the dye. However, the introduction of specific chemical moiety led to the vectorization and accumulation of the CinNapht in specific cell organelles. The Figure 7b evidently shows that the intracellular compartmentalization of the CinNaphts **6g**, **6h** and **6k** is different, also colocalization experiments were then conducted. We could easily observe a strong correlation between the fluorescence signal of the CinNapht **6g** and the lysosome tracker LysoView™ 405 confirming the accumulation of the CinNapht **6g** within the lysosome (Pearson Correlation Coefficient (PCC) = 0.91). The same conclusion was drawn when comparing the localisation of CinNapht **6k** signal with a plasma cell membrane selective dye (CellBrite® Green) with a PCC of 0.88. Finally, nuclear labeling experiments performed with compound **6k** revealed a lack of signal homogeneity from one cell to another. Nevertheless, and

regardless of the signal intensity, we observe exclusively a nuclear labelling. This was confirmed with localization experiments showing a strong spatial correspondence with NucSpot® Live 488 Nuclear Stain and a PCC of 0.89. Note that despite strong efforts devoted in finding appropriate conditions for cell imaging using CinNaphts **6i** and **6j**, by changing dye concentration or incubation time, we could not achieve selective mitochondria imaging. The images presented in Figure S9 seems to indicate that both of these dyes are sequestered in either endosome or membrane and do not enter properly in the cells, and as a consequence can not reach the mitochondria. This is important information attesting that the introduction of a cationic moiety, either pyridinium or triphenylphosphonium, does not constitutes a systematic and safe way to target mitochondria. In closing, while the former strategy required the complete resynthesis of fluorophores in order to produce fluorescent markers for a given organelle, the late stage functionalization proposed in this paper



allows to use a single step that can be considered, at will, only a few days before the imaging experiment

Investigation and use of AIEE behaviour CinNapht 5m for “wash-free” selective imaging of lipid droplets

The introduction of a diphenylamine moiety as a donating group in ICT type fluorophores often leads to a change of behavior through aggregation.²³ Thus, we looked at the emission spectra of the CinNapht **5m** in different mixtures in which the percentage of water was regularly increased within a THF/H₂O

mixture. We noticed a significant emission intensity, in THF that brutally drop when 20% of water was added (Fig. 8a). Interestingly, the intensity increased from 80% of water reaching its maximum in 99% of water. This phenomenon is also evidenced by a substantial increase of the fluorescence quantum yield from $QY_{Fl} = 0.02$ in THF to $QY_{Fl} = 0.04$ in H₂O. This typical “Aggregation-Induced Emission Enhancement” (AIEE) behavior is well illustrated by the picture reported in Figure 8b, and in the best of our knowledge, this is the first example of such behavior with CinNaphs dyes.

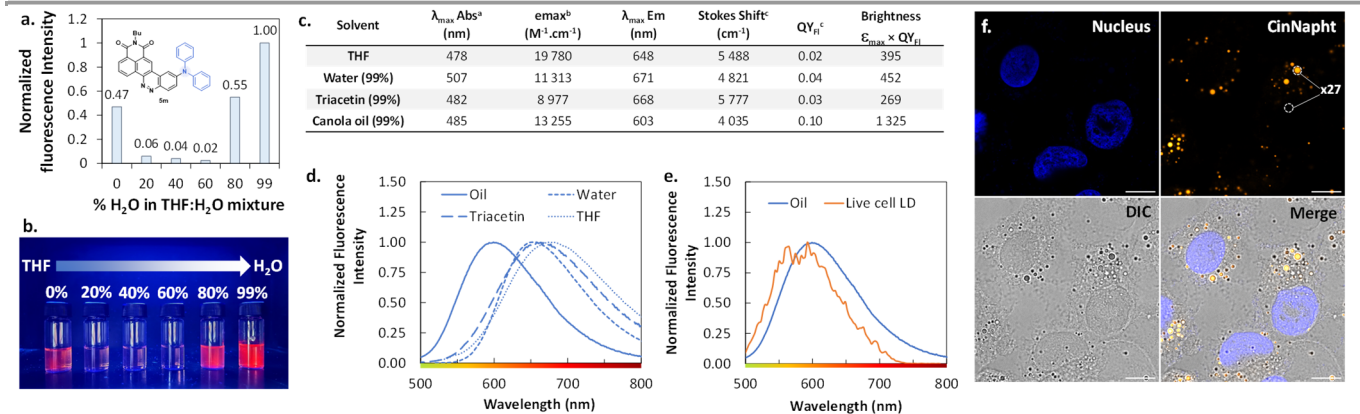


Figure 8. AIEE behaving triphenylamine analogue of CinNapht **5m**. **a.** Fluorescence Intensity of CinNapht **5m** in solution at 10^{-5} M in different THF/H₂O mixtures with different percentage of H₂O, normalized to the maximum sample Intensity (λ_{exc} : 490 nm) **b.** Photography of the CinNapht **5m** 10^{-5} M solutions under illumination at 365 nm. **c.** Table with photophysical properties of CinNapht **5m** in different media. **d.** Superposition of normalized emission spectra of CinNapht **5m** in different media. **e.** Emission spectrum recorded in living cell lipid droplets **f.** Imaging of CinNaphs **5a** using a 63x oil immersion objective, nucleus was stained with Hoechst 33342, $1\mu g/mL$ for 20 min at 37 °C (λ_{Exc} : 405 nm, λ_{Em} : 425 to 500 nm), CinNapht **5m** incubated at $5\mu M$ for 3 h at 37 °C (λ_{Exc} : 470 nm, λ_{Em} : 550 to 700 nm). Turn-on factor represent average of $n = 20$ measurements. Scale bar $10\mu M$.

We then incubated the CinNapht **5m** at $5\mu M$ with A459 living cells and studied the intracellular biodistribution of the dye. CinNapht **5m** accumulates selectively in lipid droplets (LD) as a result of what the local concentration increase leading to the aggregation of the dye resulting in a orange emission appearance as we can see in Figure 8f.²⁴ What is important to notice is that **5m** exhibit a very high signal-to-noise ratio (calculated to x27), and this without needing any wash steps. Note that LD labelling could also observed with lower concentration (up to $0.2\mu M$), showing nonetheless lower signal-to-noise ratio. We performed photophysical characterization of compound **5m** in different media including triacetin and oil in order to mimic the lipid droplet content (Fig. 8c and 8d). The best brightness was measured in canola oil. This is coherent with the observations made showing high signal selectively localized in LDs. Moreover, the measurement of the emission spectrum in the living cells LDs shows an emission centred around 580-590 nm which is close to the values measured in canola oil, (Figure 8e). Altogether, these data demonstrate that CinNapht **5m** constitutes a powerful example of an orange-emitting wash-free probe for lipid droplet imaging in living cells that were easily obtained in only one step.

Conclusions

To summarize, we propose a new and much more efficient method of access to CinNaphs that unlocks the potential of these dyes as imaging tools. This strategy is based on the late

stage introduction of the donor amine by aromatic nucleophilic substitution on a highly stable fluorinated CinNapht which can be synthesized on a large scale. This allows us to store it for a considerable period of time and to utilize it for the insertion of a wide variety of nucleophiles as we have demonstrated with the scope of the reaction. We have succeeded in developing a number of new CinNaphs that have offered access to new and more efficient organelle markers as well as photostable regioselectively deuterated derivatives. We believe that this will allow us in the future to consider more sophisticated CinNaphs based imaging tools dedicated to the study of more complex biological problems. More generally, this strategy should be applicable to other families of fluorophores, thus this work could inspire the development of a number of fluorophores based on other fluorescent polyaromatic skeletons.

Author Contributions

Chemical synthesis and characterization was performed by E. T. and M-D. H. with participation of K. T for deuteration part and B. K. for mannose functionalization. E. T. analyzed the photophysical properties. and E. V-E. performed single crystal X-ray analysis and interpreted the structural data. Theoretical calculation and interpretation of the data were performed by G. P. who also participated to the writing of the manuscript. Fluorescence microscopy and cell culture was performed A. C who also supervised the project and wrote the manuscript. All authors have given correction and approval to the final version of the manuscript.



Conflicts of interest

There are no conflicts to declare.

Acknowledgements

This project has received funding by the French National Research Agency under the program CHARMMAT ANR-11-LABX-0039-grant and with the support of the "Chemistry graduate school of Université Paris-Saclay. We also thank the Institut de Chimie des Substances Naturelles for their financial support. The present work has benefited from Imagerie-Gif light microscopy core facility supported by French National Research Agency (ANR-11-EQPX-0029/Morphoscope, ANR-10-INBS-04/FranceBioImaging ; ANR-11-IDEX-0003-02/ Saclay Plant Sciences). The University Paris-Saclay and the CNRS are acknowledged for funding. GP thanks CEA, SCBM and the European Union's Horizon 2020 research and innovation program under the FET-OPEN Grant Agreement No. 862179 for funding K.T. This work was granted access to the CCRT High-Performance Computing (HPC) facility under the Grant CCRT2023-gpieters awarded by the Fundamental Research Division (DRF) of CEA.

Notes and references

1. a) C. P. Toseland, *J. Chem. Biol.*, 2013, **6**, 85;b) M. S. T. Gonçalves, *Chem. Rev.*, 2009, **109**, 190;c) J. B. Grimm and L. D. Lavis, *Nat. Meth.*, 2022, **19**, 149.
2. a) J. Zhou and H. Ma, *Chem. Sci.*, 2016, **7**, 6309;b) L. D. Lavis and R. T. Raines, *ACS Chem. Biol.*, 2008, **3**, 142;c) J. Chan, S. C. Dodani and C. J. Chang, *Nat. Chem.*, 2012, **4**, 973;d) J. B. Grimm, L. M. Heckman and L. D. Lavis, *Prog. Mol. Biol. Transl. Sci.*, 2013, **113**, 1.
3. a) M. Más-Montoya, M. F. Montenegro, A. Espinosa Ferao, A. Tárraga, J. N. Rodríguez-López and D. Curiel, *Org. Lett.*, 2020, **22**, 3356;b) E. M. Santos, W. Sheng, R. Esmatpour Salmani, S. Tahmasebi Nick, A. Ghanbarpour, H. Gholami, C. Vasileiou, J. H. Geiger and B. Borhan, *J. Am. Chem. Soc.*, 2021, **143**, 15091;c) A. Gandioso, R. Bresoli-Obach, A. Nin-Hill, M. Bosch, M. Palau, A. Galindo, S. Contreras, A. Rovira, C. Rovira, S. Nonell and V. Marchán, *J. Org. Chem.*, 2018, **83**, 1185;d) J.-A. Richard, M. Massonneau, P.-Y. Renard and A. Romieu, *Org. Lett.*, 2008, **10**, 4175;e) L. Zhou, Q. Wang, Y. Tan, M. J. Lang, H. Sun and X. Liu, *Chem. Eur. J.*, 2017, **23**, 8736;f) X. Zhang, J. Wang, F. Yu, X. Huang, N. Wang, T. Wang and H. Hao, *Cryst. Growth Des.*, 2022, **22**, 3198;g) I. Likhokin, R. Lincoln, M. L. Bossi, A. N. Butkevich and S. W. Hell, *J. Am. Chem. Soc.*, 2023, **145**, 1530;h) A. Gandioso, R. Bresoli-Obach, A. Nin-Hill, M. Bosch, M. Palau, A. Galindo, S. Contreras, A. Rovira, C. Rovira, S. Nonell and V. Marchán, *J. Org. Chem.*, 2018, **83**, 1185;i) L. Yuan, W. Lin, S. Zhao, W. Gao, B. Chen, L. He and S. Zhu, *J. Am. Chem. Soc.*, 2012, **134**, 13510.
4. M.-D. Hoang, J.-B. Bodin, F. Savina, V. Steinmetz, J. Bignon, P. Durand, G. Clavier, R. Méallet-Renault and A. Chevalier, *RSC Adv.*, 2021, **11**, 30088.
5. M.-D. Hoang, F. Savina, P. Durand, P. R. Méallet-Renault, G. Clavier and A. Chevalier, *ChemPhotoChem*, 2022, **6**, e202200138.
6. a) J. B. Grimm, A. J. Sung, W. R. Legant, P. Hulamm, S. M. Matlosz, E. Betzig and L. D. Lavis, *ACS Chem. Biol.*, 2013, **8**, 1303;b) S. M. Hickey, S. O. Nitschke, M. J. Sweetman, C. J. Sumbly, D. A. Brooks, S. E. Plush and T. D. Ashton, *J. Org. Chem.*, 2020, **85**, 7986;c) J. B. Grimm and L. D. Lavis, *Org. Lett.*, 2011, **13**, 6354;d) S. C. O. Uy, C. Uttamapinant and A. Y. Ting, *ChemBioChem*, 2011, **12**, 65;e) T. Peng and D. Yang, *Org. Lett.*, 2010, **12**, 496;f) K. N. Hearn, T. D. Nalder, R. P. Cox, H. D. Maynard, T. D. M. Bell, F. M. Pfeffer and T. D. Ashton, *Chem. Commun.*, 2017, **53**, 12298.
7. a) J. B. Grimm, A. K. Muthusamy, Y. Liang, T. A. Brown, W. C. Lemon, R. Patel, R. Lu, J. J. Macklin, P. J. Keller, N. Ji and L. D. Lavis, *Nat. Meth.*, 2017, **14**, 987;b) J. B. Grimm, L. Xie, J. C. Casler, R. Patel, A. N. Tkachuk, N. Falco, H. Choi, J. Lippincott-Schwartz, T. A. Brown, B. S. Glick, Z. Liu and L. D. Lavis, *JACS Au*, 2021, **1**, 690;c) A. N. Butkevich, M. L. Bossi, G. Lukinavičius and S. W. Hell, *J. Am. Chem. Soc.*, 2019, **141**, 981.
8. a) J. Bucevičius, G. Kostiuk, R. Gerasimaitė, T. Gilat and G. Lukinavičius, *Chem. Sci.*, 2020, **11**, 7313;b) C. Deo, A. S. Abdelfattah, H. K. Bhargava, A. J. Berro, N. Falco, H. Farrant, B. Moeyaert, M. Chupanova, L. D. Lavis and E. R. Schreiter, *Nat. Chem. Biol.*, 2021, **17**, 718;c) T. Takagi, T. Ueno, K. Ikawa, D. Asanuma, Y. Nomura, S.-n. Uno, T. Komatsu, M. Kamiya, K. Hanaoka, C. Okimura, Y. Iwadate, K. Hirose, T. Nagano, K. Sugimura and Y. Urano, *Sci. Adv.*, 2021, **7**, eabg8585;d) J. M. Meinig, L. Fu and B. R. Peterson, *Angew. Chem. Int. Ed.*, 2015, **54**, 9696.
9. a) W. Shi, J. Li, X. He, S. Zhou, H. Sun and H. Wu, *Org. Lett.*, 2022, **24**, 3368;b) M. Motoyama, T.-H. Doan, P. Hibner-Kulicka, R. Otake, M. Lukarska, J.-F. Lohier, K. Ozawa, S. Nanbu, C. Alayrac, Y. Suzuki and B. Witulski, *Chem. Asian J.*, 2021, **16**, 2087;c) G. Zhang, M. Wang, P. Bobadova-Parvanova, F. R. Fronczek, K. M. Smith and M. G. H. Vicente, *Chem. Eur. J.*, 2022, **28**, e202200421;d) S. Zheng, G. Lingyue, M. J. H. Ong, D. Jacquemin, A. Romieu, J.-A. Richard and R. Srinivasan, *Org. Biomol. Chem.*, 2019, **17**, 4291;e) G. Vives, C. Giansante, R. Bofinger, G. Raffy, A. D. Guerzo, B. Kauffmann, P. Batat, G. Jonusauskas and N. D. McClenaghan, *Chem. Commun.*, 2011, **47**, 10425;f) M. Kotaskova, O. Osman Oglou and M. Helm, *Org. Biomol. Chem.*, 2014, **12**, 3816;g) A. Chevalier, K. Renault, F. Boschetti, P.-Y. Renard and A. Romieu, *Eur. J. Org. Chem.*, 2015, **2015**, 152.
10. a) H.-R. Jia, Y.-X. Zhu, Q.-Y. Duan and F.-G. Wu, *Chem. Soc. Rev.*, 2021, **50**, 6240;b) P. Shieh, V. T. Dien, B. J. Beahm, J. M. Castellano, T. Wyss-Coray and C. R. Bertozzi, *J. Am. Chem. Soc.*, 2015, **137**, 7145.
11. a) H. A. Henthorn and M. D. Pluth, *J. Am. Chem. Soc.*, 2015, **137**, 15330;b) V. S. Lin, W. Chen, M. Xian and C. J. Chang, *Chem. Soc. Rev.*, 2015, **44**, 4596.
12. G. Zhou, S. Hou, N. Zhao, N. Finney and Y. Wang, *Dyes Pigm.*, 2022, **204**, 110394.
13. a) V. V. Rostovtsev, L. G. Green, V. V. Fokin and K. B. Sharpless, *Angew. Chem. Int. Ed.*, 2002, **41**, 2596;b) C. W. Tornøe, C. Christensen and M. Meldal, *J. Org. Chem.*, 2002, **67**, 3057.
14. a) L. Wang, Y. Xiao, W. Tian and L. Deng, *J. Am. Chem. Soc.*, 2013, **135**, 2903;b) H. Yu, Y. Xiao and L. Jin, *J. Am. Chem. Soc.*, 2012, **134**, 17486;c) Q. Wan, S. Chen, W. Shi, L. Li and H. Ma, *Angew. Chem. Int. Ed.*, 2014, **53**, 10916.
15. D. I. Danylchuk, P.-H. Jouard and A. S. Klymchenko, *J. Am. Chem. Soc.*, 2021, **143**, 912.
16. a) Z. Xu and L. Xu, *Chem. Commun.*, 2016, **52**, 1094;b) Roopa, N. Kumar, V. Bhalla and M. Kumar, *Chem. Commun.*, 2015, **51**, 15614;c) S. Samanta, Y. He, A. Sharma, J. Kim, W. Pan, Z. Yang, J. Li, W. Yan, L. Liu, J. Qu and J. S. Kim, *Chem*, 2019, **5**, 1697;d) J. Zielonka, J. Joseph, A. Sikora, M. Hardy, O. Ouari, J. Vasquez-Vivar, G. Cheng, M. Lopez and B. Kalyanaraman, *Chem. Rev.*, 2017, **117**, 10043;e) R. A. J. Smith, C. M. Porteous, A. M. Gane and M. P. Murphy, *Proc. Nat. Ac. Sci.*, 2003, **100**, 5407.



17. a) A. Nakamura, K. Takigawa, Y. Kurishita, K. Kuwata, M. Ishida, Y. Shimoda, I. Hamachi and S. Tsukiji, *Chem. Commun.*, 2014, **50**, 6149; b) C. K. Spahn, M. Glaesmann, J. B. Grimm, A. X. Ayala, L. D. Lavis and M. Heilemann, *Scientific Reports*, 2018, **8**, 14768.
18. K. Roßmann, K. C. Akkaya, P. Poc, C. Charbonnier, J. Eichhorst, H. Gonschior, A. Valavalkar, N. Wendler, T. Cordes, B. Dietzek-Ivanšić, B. Jones, M. Lehmann and J. Broichhagen, *Chem. Sci.*, 2022, **13**, 8605.
19. E. Levernier, K. Tatoueix, S. Garcia-Argote, V. Pfeifer, R. Kiesling, E. Gravel, S. Feuillastre and G. Pieters, *JACS Au*, 2022, **2**, 801.
20. K. Rurack and M. Spieles, *Anal. Chem.*, 2011, **83**, 1232.
21. <https://www.atto-tec.com/product-141-142.html?language=de>).
22. <https://www.thermofisher.com/order/catalog/product/fr/fr/82491>).
23. a) D. Wang and B. Z. Tang, *Acc. Chem. Res.*, 2019, **52**, 2559; b) Y. Lin, Y. Song, Y. Jin, B. Wang and C. Fan, *Dyes Pigm.*, 2020, **183**, 108711; c) K. Zhang, J. Shu, W. Chu, X. Liu, B. Xu and W. Jiang, *Dyes Pigm.*, 2021, **185**, 108898.
24. L. Wang, X. Chen, X. Ran, H. Tang and D. Cao, *Dyes Pigm.*, 2022, **203**, 110332.

View Article Online
DOI: 10.1039/D3SC01365K

